

Applications of electrostatic capacitance and charging

Titus Sandu,¹ George Boldeiu,² and Victor Moagar-Poladian²

¹*National Institute for Research and Development in Microtechnologies-IMT,
126A, Erou Iancu Nicolae Street, 077190, Bucharest, ROMANIA**

²*National Institute for Research and Development in Microtechnologies-IMT,
126A, Erou Iancu Nicolae street, 077190, Bucharest, ROMANIA*

(Dated: January 9, 2014)

The capacitance of an arbitrarily shaped object is calculated with the same second-kind integral equation method used for computing static and dynamic polarizabilities. The capacitance is simply the dielectric permittivity multiplied by the area of the object and divided by the squared norm of the Neumann-Poincaré operator eigenfunction corresponding to the largest eigenvalue. The norm of this eigenfunction varies slowly with shape thus enabling the definition of two scale-invariant shape factors and perturbative calculations of capacitance. The result is extended to a special class of capacitors in which the electrodes are the equipotential surfaces generated by the equilibrium charge on the object. This extension allows analytical expressions of capacitance for confocal spheroidal capacitors and finite cylinders. Moreover, a second order formula for thin constant-thickness capacitors is given with direct applications for capacitance of membranes in living cells and of supercapacitors. For axisymmetric geometries a fast and accurate numerical method is provided.

PACS numbers: 41.20.Cv, 82.47.Uv, 87.19.rf, 87.50.C-

I. INTRODUCTION

Potential theory has been proved very successfully in solving some boundary value problems such as the Dirichlet and the Neumann problems or the electrostatic charge distribution on conductors. For domains with sufficiently smooth boundaries (i.e., a regular piecewise Lyapunov surface) the above problems use specific types of potentials like the volume, the single-, and the double-layer potentials, the logarithmic potential for two-dimensional domains, etc.^{1,2}. The Dirichlet and Neumann problems defined on domains with sufficiently smooth boundaries can be recast in integral equations which lead to compact operators on domain boundary: the Neumann-Poincaré (or double-layer) operator and its adjoint². These methods are applied in some practical and physical problems regarding dielectric heterogeneous systems like the radio-frequency and microwave dielectric spectra of living cells³ and plasmonic properties of metallic nanoparticles^{4,5}. Another problem is the equilibrium charge distribution on a conductor (the Robin problem)⁶ and the implicit capacitance with applications in computational biophysics⁷, in scanning probe microscopy^{8,9}, or in electrical charge storage in supercapacitors¹⁰.

The capacitance of an arbitrarily shaped body is calculated by “mimicking” some directly related phenomena like the diffusion-controlled reactions¹¹ or the ergodic generation of the equilibrium charge distribution¹². The standard procedures for solving the Laplace equation are the Finite Element Method (FEM)¹³ or the Boundary Integral Equation (BIE) method with the finite element formulation as the Boundary Element Method (BEM)¹⁴. In contrast to the FEM, in the BEM only the surfaces of the inclusions are discretized, such that with numerical algorithms like the fast multipole method (FMM) of Rokhlin and Greengard^{15,16} the calculations are essen-

tially of $O(N)$, where N is the number of nodes. The capacitance of an arbitrary object has been treated in different contexts with $O(N)$ FMM schemes (see Ref. 17 and the references therein). It can be treated as a first-¹⁸ or as a second-kind integral equation. The second-kind integral formulation is based either on the Neumann-Poincaré operator¹⁹ or on its adjoint¹⁷. The most convenient approach is, however, the second-kind integral equation with the adjoint of the Neumann-Poincaré operator which provides both the charge density and the capacitance¹⁷.

In this paper we adopt such a BIE method to calculate the capacitance and the equilibrium charge on an arbitrarily shaped object with several applications. The capacitance is obtained concurrently with other physical properties like the static and the dynamic polarizabilities of nanoparticles with applications in nanoparticle manipulation²⁰ and plasmonics⁵. We use a spectral method²¹⁻²³ which provides an exponential convergence²⁴. Moreover, our basis functions include spherical harmonics²¹ that can be directly related with the multipoles in the FMM of Rokhlin^{15,16}. Compared to others the present method shows directly that the geometric dependence of capacitance is incorporated in a norm of a given eigenvector of the Neumann-Poincaré operator. This eigenvector norm varies slowly with the geometry hence two scale-invariant defined shape factors can be readily used in the estimation of capacitance for arbitrary shapes. Furthermore, we define a specific class of capacitors in which the electrodes are the equipotential surfaces generated by the equilibrium charge on an arbitrarily shaped metallic object with applications regarding some analytical results like confocal spheroidal capacitors and finite cylinders. We also provide a second order compact capacitance formula for thin and constant-thickness capacitors with other applications referring to

membrane capacitance of living cells and charge storage in supercapacitors.

The paper is organized as follows. In the second section we define the capacitance in the second-kind integral form. Then, we define a general capacitor and a specific class of capacitors in the following section. Section 4 describes the numerical method and the applications just mentioned above. A summary is given in the last section.

II. CAPACITANCE OF A METALLIC OBJECT IN A SECOND-KIND INTEGRAL FORMULATION

We assume an arbitrarily shaped domain Ω bounded by the surface Σ in the 3-dimensional space. The following operators can be defined on Σ : \hat{M} , its adjoint \hat{M}^\dagger , and \hat{S} .^{1,2} The action of \hat{M} on a function u signifies the normal electric field to Σ generated by the charge density u . The operator \hat{M}^\dagger , which is the Neumann-Poincaré (or double-layer) operator, acts on the dipole density v generating an electric potential on Σ . On the other hand, \hat{S} is a Coulomb (single-layer) operator which acts on the charge density u creating an electric potential on Σ .

The operators \hat{M} and \hat{M}^\dagger have the same spectrum within $-1/2$ and $1/2$ and the eigenfunctions u_i of \hat{M} are related to the eigenfunctions v_i of \hat{M}^\dagger by $v_i = \hat{S}[u_i]$, which makes them bi-orthogonal, i.e., $\langle v_j | u_i \rangle = \delta_{ij}$.²³ The largest eigenvalue of \hat{M} and \hat{M}^\dagger is $1/2$ irrespective of the domain shape^{2,21} and the corresponding eigenfunction v_1 of \hat{M}^\dagger is a constant function, i. e., $v_1 = \text{constant}$ on Σ . As we will discuss below, the companion eigenfunction u_1 of \hat{M} is proportional to the equilibrium charge distribution on a conductor of shape determined by Σ . We note that the spectrum of \hat{M} and \hat{M}^\dagger is scale invariant, but the spectrum of \hat{S} is proportional to the linear size of Ω .

\hat{M} and \hat{S} can be used in the resolution of many physical problems like the static²⁰ or the dynamic object polarizability represented by the dielectric spectra of living cells^{3,21} or the optical properties of metallic nanoparticles^{4,5,22,23}. Another closely related issue is the Robin problem of finding the equilibrium charge distribution u_R on a conductor of arbitrary shape⁶. It can be cast into an integral equation of the second-kind that has the operator form

$$\hat{M}[u_R] = \frac{1}{2}u_R(\mathbf{x}), \quad (1)$$

with the constraint $\int_{\mathbf{x} \in \Sigma} u_R(\mathbf{x})d\Sigma(\mathbf{x}) = 1$. The constraint can be put in the following form $\langle 1 | u_R \rangle = 1$, where 1 is the constant function of value 1 on Σ . Equation (1) has the obvious solution $u_R \propto u_1$. The constant value V_R of the electric potential generated by u_R is formally given by $\hat{S}[u_R] = V_R 1$ and is called the Robin constant, while its inverse is the capacitance C of the body bounded by Σ . If we consider the dielectric permittivity ε of

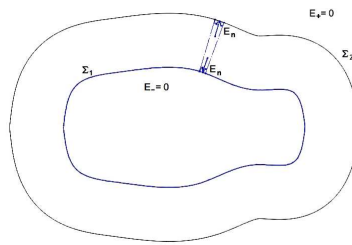


FIG. 1: Schematic representation of a capacitor with the configurations of fields inside Σ_1 and outside Σ_2 . The dotted lines delimitate a Gaussian surface used in the text.

the embedding medium and the constraint $\langle 1 | u_R \rangle = 1$ the capacitance is $C = \varepsilon / \langle u_R | \hat{S}[u_R] \rangle$. Furthermore, if $u_R = a_1 u_1$, one can prove that the constant a_1 is the proportionality factor between v_1 and the constant distribution 1, i. e., $1 = v_1 / a_1$. Then we can relate a_1 to the norm of v_1 by the following chain of equations $\langle v_1 | v_1 \rangle = \|v_1\|^2 = a_1^2 \langle 1 | 1 \rangle = a_1^2 A$, where A is the area of Σ . Finally, the capacitance takes a simple and compact form

$$C = \frac{\varepsilon A}{\|v_1\|^2}. \quad (2)$$

One can show that $\|v_1\|^2$ is proportional to the linear size of Ω therefore, the capacitance itself is also proportional to the linear size of the body. Equation (2) shows explicitly both the geometric dependence of capacitance of an arbitrarily shaped object and the scale invariance of the shape factor $C/\sqrt{4\pi A}$. The shape factor varies slowly with the conductor shape²⁵ hence, as we will discuss in the next section, $\|v_1\|^2$ is a slowly varying function of the conductor shape and perturbative estimations of capacitance can be performed.

III. CAPACITORS AND THEIR CAPACITANCE

A. Definition

In general, a capacitor consists of two separated conducting bodies. We consider a capacitor that is made of two smooth surfaces Σ_1 and Σ_2 in which Σ_2 encloses Σ_1 (Fig. 1). The capacitance of the capacitor is defined as the total charge that is held on Σ_1 when the electrical potential is 1 on Σ_1 and 0 on Σ_2 . Therefore, the electrostatic problem is the Laplace equation in the space Ω_{12} between Σ_1 and Σ_2 :

$$\Delta u(\mathbf{x}) = 0; \quad \mathbf{x} \in \Omega_{12} \quad (3)$$

with the boundary conditions $u(\mathbf{x}) = 1$ for $\mathbf{x} \in \Sigma_1$ and $u(\mathbf{x}) = 0$ for $\mathbf{x} \in \Sigma_2$. It is easy to see that with these boundary conditions the solution of the Laplace equation inside of Σ_1 and outside of Σ_2 is the constant 1 and the

constant 0, respectively. Inside Ω_{12} we seek a solution for (3) in the form of two single-layer potentials

$$u(x) = \int_{\mathbf{y} \in \Sigma_1} \frac{\mu_1(\mathbf{y})}{4\pi |\mathbf{x} - \mathbf{y}|} d\Sigma(\mathbf{y}) + \int_{\mathbf{y} \in \Sigma_2} \frac{\mu_2(\mathbf{y})}{4\pi |\mathbf{x} - \mathbf{y}|} d\Sigma(\mathbf{y}), \quad (4)$$

where μ_1 and μ_2 are the induced charge densities on Σ_1 and Σ_2 . Similar to \hat{M} and \hat{S} we define on Σ_1 and Σ_2 four operators \hat{M}_{ij} and four operators \hat{S}_{ij} as follows

$$\hat{M}_{ij}[\mu_j] = \int_{\mathbf{x} \in \Sigma_i, \mathbf{y} \in \Sigma_j} \frac{\mu_j(\mathbf{y}) \mathbf{n}(\mathbf{x}) \cdot (\mathbf{x} - \mathbf{y})}{4\pi |\mathbf{x} - \mathbf{y}|^3} d\Sigma(\mathbf{y}), \quad (5)$$

$$\hat{S}_{ij}[u] = \int_{\mathbf{x} \in \Sigma_i, \mathbf{y} \in \Sigma_j} \frac{u(\mathbf{y})}{4\pi |\mathbf{x} - \mathbf{y}|} d\Sigma(\mathbf{y}), \quad (6)$$

with $i, j = \overline{1, 2}$. In Eq. (5) \mathbf{n} is the normal vector to $\Sigma_{1,2}$. The equations obeyed by μ_1 and μ_2 are

$$\begin{aligned} \hat{M}_{11}[\mu_1] + \hat{M}_{12}[\mu_2] &= \frac{1}{2}\mu_1 \\ \hat{M}_{21}[\mu_1] + \hat{M}_{22}[\mu_2] &= -\frac{1}{2}\mu_2 \\ \hat{S}_{11}[\mu_1] + \hat{S}_{12}[\mu_2] &= 1 \\ \hat{S}_{21}[\mu_1] + \hat{S}_{22}[\mu_2] &= 0. \end{aligned} \quad (7)$$

The first two equations of (7) set the normal fields on Σ_1 from inside and on Σ_2 from outside to zero, while the last two equations are the boundary conditions of (3). The solution of the first two equations in (7) is the solution of (3) up to multiplicative constants. The multiplicative constants are fixed by the last two equations of (7).

B. A special class of capacitors

The capacitance of the capacitor is the total charge on Σ_1 and depends on inter-surface operators \hat{M}_{ij} and \hat{S}_{ij} . In the special case when Σ_2 is an equipotential surface determined by the equilibrium charge distributed on Σ_1 a compact capacitance formula can be deduced with the help of \hat{M} and \hat{S} only. It is not hard to see that solutions μ_1 and μ_2 of the first two equations of (7) are proportional to the equilibrium charge densities on Σ_1 and Σ_2 , respectively. To determine μ_1 and μ_2 one needs the boundary conditions given by the last two equations of (7). Thus, by integrating the third equation of (7) on Σ_1 and the fourth equation on Σ_2 one obtains the following relations $V_1 + V_2 = 1$ and $V_{12} + V_2 = 0$, where V_1 is the electric potential induced by μ_1 on Σ_1 , V_2 is the electric potential induced by μ_2 inside Σ_2 as well as on Σ_1 , and V_{12} is the electric potential induced on Σ_2 by μ_1 . On the other hand, the total charges on Σ_1 and on Σ_2 are $Q_1 = C_1 V_1$ and $Q_2 = C_2 V_2$, which are valid only if Σ_2 is one of the equipotential surfaces determined by an equilibrium charge distributed on Σ_1 . Equation (2)

provides the expressions of C_1 and C_2 that are the capacitances of Σ_1 and Σ_2 , respectively. Keeping in mind that $Q_1 + Q_2 = 0$ we obtain the capacitance

$$C_{cond} = \left(\frac{1}{C_1} - \frac{1}{C_2} \right)^{-1}. \quad (8)$$

In the limiting case of very thin capacitors (i. e., Σ_2 being very close to Σ_1) Eq. (8) takes a planar-like capacitor expression given by

$$C_{thin_capacitor} = \varepsilon \int_{\mathbf{y} \in \Sigma} \frac{d\Sigma(\mathbf{y})}{\delta d}, \quad (9)$$

where δd is the "distance" between Σ_1 and Σ_2 locally defined below. In the vicinity of Σ_1 a coordinate system $(\zeta_1, \zeta_2, \zeta_3)$ can be defined, such that ζ_1 and ζ_2 describe Σ_1 while ζ_3 is the electric potential following the field lines from Σ_1 to Σ_2 . The electric potential V_2 on Σ_2 is related to V_1 , the electric potential on Σ_1 , by

$$V_2 \cong V_1 + \frac{\partial V}{\partial \zeta_3} \delta \zeta_3, \quad (10)$$

where $\delta \zeta_3$ is a small variation of ζ_3 from Σ_1 to Σ_2 . The local thickness of the capacitor is $\delta d = h_{\zeta_3} \delta \zeta_3$, with h_{ζ_3} as the Lamé coefficient corresponding to ζ_3 ²⁶. From Eq. (10) Gauss theorem (see for instance Fig. 1) provides the charge density $\sigma = \varepsilon(V_1 - V_2)/\delta d$. Integrating the charge σ over Σ_1 and dividing by $V_1 - V_2$ one obtains (9). Now we consider without loss of generality that $(\zeta_1, \zeta_2, \zeta_3)$ is orthogonal. Then using Eq. (9) the form of Eq. (8) can be recast as

$$C_{cond} = \varepsilon \left(\int_1^0 \frac{d\zeta_3}{\int_{\mathbf{y} \in \Sigma} \frac{d\Sigma(\mathbf{y})}{h_{\zeta_3}(\mathbf{y})}} \right)^{-1}. \quad (11)$$

The validity of (9) is more general than that of the case considered above (in which Σ_2 is an equipotential surface generated by the equilibrium charge on Σ_1). Some examples will be provided in the next section, where it will be also discussed cases in which (9) may not be good enough.

Particular examples of Eqs. (8) and (11) are the capacitances of concentric spheres and of coaxial cables. For a capacitor made of two concentric spheres the capacitance is $C_{sph_cond} = 4\pi\varepsilon R_1 R_2 / (R_2 - R_1)$, where R_1 and R_2 are the radii of the two spheres with $R_2 > R_1$. Since the capacitance of a sphere is $C_{sph} = 4\pi\varepsilon R$, it is easy to check that C_{sph_cond} has the form given by Eq. (8).

The capacitance of a capacitor made of two confocal spheroids obeys also (8) and can be calculated with Eq. (11). Two confocal spheroids are conveniently described in spheroidal coordinates (η, ξ, φ) , which for prolate spheroids obey the equations

$$\begin{aligned} x &= c\sqrt{\eta^2 - 1}\sqrt{1 - \xi^2} \cos(\varphi) \\ y &= c\sqrt{\eta^2 - 1}\sqrt{1 - \xi^2} \sin(\varphi) \\ z &= c\eta\xi. \end{aligned} \quad (12)$$

The two confocal spheroids defining Σ_1 and Σ_2 are determined by $\eta = \eta_1$ and $\eta = \eta_2$, respectively. The coordinates (η, ξ, φ) are orthogonal and it can be shown that the equipotential surfaces of the equilibrium charge on the spheroid of equation $\eta = \eta_1$ is any confocal spheroid of equation $\eta = \eta_2 > \eta_1$ ²⁶. From Eq. (11) one obtains directly the capacitance of a confocal spheroidal capacitor as in the following expression

$$C_{\text{prolate_capacitor}} = \frac{4\pi\epsilon c}{Q_0^0(\eta_1) - Q_0^0(\eta_2)}, \quad (13)$$

where $Q_0^0(\eta) = \ln((\eta+1)/(\eta-1))$. Eq. (13) is of form (8) since the capacitance of a prolate spheroid alone ($\eta_2 \rightarrow \infty$) is $C_{\text{prolate_spheroid}} = 4\pi\epsilon c/Q_0^0(\eta_1)$ which is given in the standard textbooks of classical electrodynamics²⁶. The capacitances of oblate confocal spheroids are found replacing η by $i\eta$ and c by $-ic$. An expression similar to (13) was found in a recent paper²⁷, where the authors did not notice the significance of Eq. (13) in terms of Eq. (11).

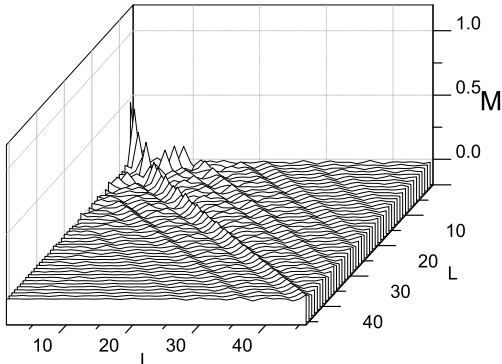


FIG. 2: Matrix elements of \hat{M} in the \tilde{Y}_{Lm} basis. The matrix indices designate the indices L of the spherical harmonics \tilde{Y}_{Lm} . For axisymmetric objects only $m = 0$ is relevant.

IV. APPLICATIONS AND DISCUSSION

A. A Numerical method

The capacitance can be determined in numerical simulators used to calculate other physical properties like the dynamic polarizabilities needed for localized plasmon resonances in metallic nanoparticles^{4,5}. Simultaneous calculations of capacitance and polarizability were also performed in the path integral formulation by averaging over random walk trajectories²⁸. Our numerical method is an operator based BIE method that calculates the eigenvalues χ_k and the eigenvectors u_k and v_k of \hat{M} and \hat{M}^\dagger , respectively. In order to have normed u_k and v_k one needs also to calculate the matrix elements of \hat{S} ²³. The present method belongs to the class of the

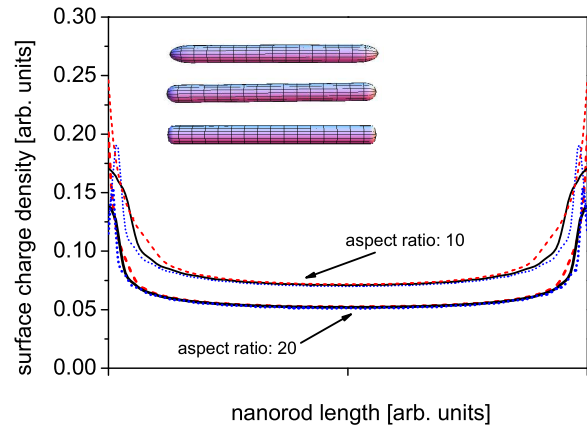


FIG. 3: (Color online) The equilibrium surface charge density on rods with various cappings shown in the inset: hemisphere (black solid line), oblate hemispheroid (blue dotted line), and prolate hemispheroid (red dashed line).

spectral methods which are fast converging²⁴. In these methods the functions of the basis set are defined globally rather than locally like in the standard FEM. In our approach the function set is related to the spherical harmonics $Y_{Lm}(\theta, \varphi)$ defined on a sphere that is related to Σ by the map $\mathbf{x} \rightarrow (\theta(\mathbf{x}), \varphi(\mathbf{x}))$. Details of the method for axisymmetric objects are given in Refs. 21,22. In Fig. 2 we plotted the matrix elements of \hat{M} for a generic axially symmetric object. It is easy to notice that the matrices are sparse with the significant matrix elements being around the diagonal or/and at low-value indices which are basically low-order multipoles. The matrix elements of \hat{S} show also a similar behavior. Thus, our method is similar to the FMM in which the major contributions come from the low-order multipoles^{15,16}. The validity of the numerical method was checked by calculations performed on oblate and prolate spheroids, which have analytical expressions discussed above. Our numerical calculations show a very good agreement with the analytical results. The relative error is at most 5×10^{-5} with a relative small overhead of 25 functions in the basis and 96 quadrature points. The implementation of BIE for axisymmetric shapes has also shown to provide very accurate results of the depolarization factors which are related to other eigenvalues of \hat{M} and \hat{M}^\dagger ²⁹.

B. Cylindrical rods

We have also performed numerical calculations on cylindrical rods with different end-cap geometries: half of an oblate spheroid with 1/2 aspect ratio, half of a sphere, and half of a prolate spheroid with an aspect ratio of 2. In Fig. 3 we have plotted the surface charge density of metallic rods with the above cappings. Two aspect ratios have been considered: 10 and 20. Since the charge preserves the axial symmetry only the lon-

itudinal dependence is shown. Fig. 3 illustrates that, ignoring the capping zones, the charge density is almost the same. The resemblance is greater as the aspect ratio becomes larger. In addition, in the middle of the rod the charge density is almost constant and decreases with the increase of the aspect ratio.

Let us now consider two hemispherically capped rods. The first one is determined by the surface Σ_1 that is a cylinder of length L and caps of radius R_1 . The other rod is determined by the outer surface Σ_2 with the same length L , but with a radius $R_2 > R_1$. Σ_1 and Σ_2 have the same normal hence, geometrical intuition tells us that we can apply Eq. (11) to obtain the capacitance of a such capacitor made of two finite cylindrical rods with hemispherical ends. Explicit numerical calculations of equipotential surfaces show that the above assumption is quite good. Therefore, by applying Eq. (11) we obtain the following expression

$$C_{rod_capacitor} = \frac{2\pi\epsilon L}{\ln\left(\frac{R_2(R_1+L/2)}{R_1(R_2+L/2)}\right)}. \quad (14)$$

Eq. (14) recovers known results in two limiting cases: (a) concentric spheres, $L \rightarrow 0$; and (b) coaxial cable, $L \rightarrow \infty$. In the limiting case of $R_2 \rightarrow \infty$ one obtains the capacitance of a finite cylindrical rod with hemispherical cappings

$$C_{hemispherical_rod} = \frac{4\pi\epsilon R_1(m-1)}{\ln(m)}, \quad (15)$$

with $m = (L + 2R_1)/(2R_1)$ as the aspect ratio of the rod.

This result can be extended to finite cylinders with hemispheroidal cappings where the equipotential surfaces are determined by the corresponding confocal spheroids. In the particular case of oblate hemispheroidal cappings one may obtain the limit of cylinder with flat cappings. Thus, after some tedious but otherwise straightforward calculations the capacity of cylinders with flat endings is

$$C_{flat_rod} = \frac{4\pi\epsilon R(m^2 + 1)}{m(\ln(m) + \frac{\pi}{2m})}, \quad (16)$$

with $m = L/(2R)$ as the aspect ratio of the rod. Here L is the length of the rod and R is its axial radius. We easily notice that for $m \rightarrow 0$ Eq. (16) reproduces the capacitance of a disk²⁶.

We have compared numerical capacitance calculations of cylindrical rods having different capping geometries (flat, oblate hemispheroidal, and hemispherical) with Eqs. (15) and (16) and with Smythe's³⁰ and Jackson's³¹ analytical results. Numerical results are obtained using either the BIE method for rods with oblate hemispheroidal and hemispherical cappings or the multiphysics program ANSYS (found at www.ansys.com) for rods with flat cappings. The results are given in Fig. 4a. The oblate hemispheroidal cappings are chosen to be thin (an aspect ratio of 10), which provides quite good approximants for cylinders with flat ends. For example, the capacitances of flat and oblate hemispheroidal

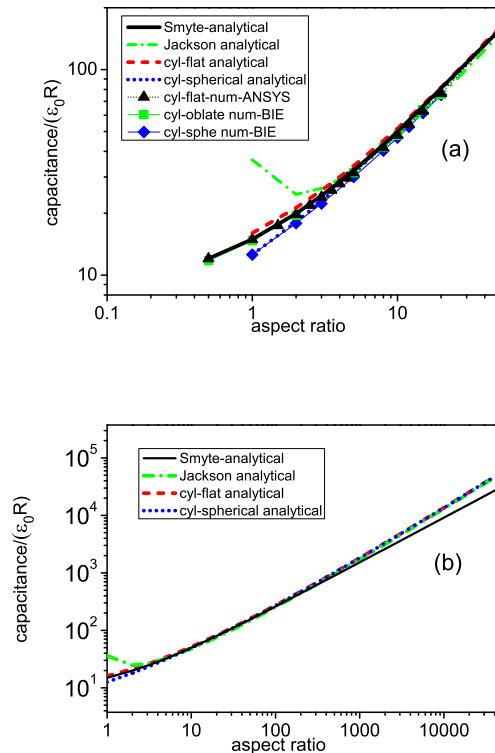


FIG. 4: (Color online) (a) Analytical and numerical calculations of capacitance for various cylindrical rods at relatively small aspect ratios. (b) Various analytical results over a sufficiently large range of aspect ratios. The capacitances are given in terms of $\epsilon_0 R$, with ϵ_0 as the vacuum permittivity and R as the cross-sectional radius.

capped cylinders are apart only by 2% at an aspect ratio of 1/2. Moreover, for aspect ratios greater than 5 the capacitance of the rods do not depend any longer on the end-cap geometry (the differences are well below 1%). On the other hand, the analytical results of Eq. (15) are apart by up to 5.5% from the BIE calculations for cylinders with hemispherical ends at the aspect ratio of 20. Furthermore, Eq. (16) is also within a few percentage points from the exact results at low aspect ratios, but at larger aspect ratios Eqs. (15) and (16) are sufficiently close. In Fig. 4b we compare Eqs. (15) and (16) with the Smythe's³⁰ and Jackson's³¹ formulae. There are known that the Smythe's formula is valid at low aspect ratios (below 10)³⁰, while the Jackson's³¹ works well at large aspect ratios. We mention that in another derivation there were obtained also two different expressions of capacitance for short and the long cylinders, respectively³². In contrast, as one can see from Fig. 4 Eqs. (15) and (16) work well for both short and the long cylinders and also have simple algebraic expressions. These results are not that surprising after all. They are asymptotically exact for $m \rightarrow 0$ and $m \rightarrow \infty$ by construction. The case of very

long cylinders was first considered by Maxwell³³, who stated that, for $m \rightarrow \infty$, the charge density tends to be constant. As proved in a separate paper³⁴ the charge and implicitly the capacitance given by Jackson³¹ are similar to those of Maxwell's (e.g., $C = 4\pi\epsilon Rm/(\ln(4m) - 1)$) which are accurate for large but not for small m 's.

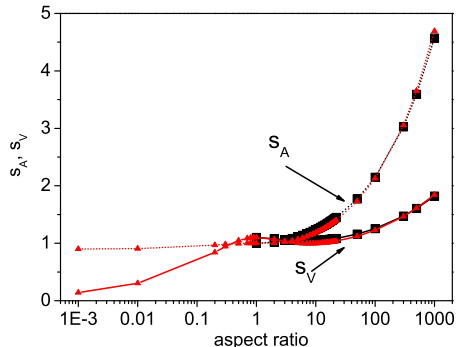


FIG. 5: (Color on-line) Scale-invariant shape factors versus aspect ratio. The shape factors are defined either by the area of the object (s_A -dotted lines with symbols) or by its volume (s_V -solid lines with symbols). The spheroids and the cylindrical rods are denoted by black squares and by red triangles, respectively.

C. Scale-invariant shape factors and some consequences

Since the capacitance is proportional to the linear size of the object one can define shape factors that are scale-invariant. For instance one can employ the surface or the volume of the object to define scale-invariant shape factors. Two of such shape factors are presented in Fig. 5 for cylinders and spheroids.

The first scale-invariant shape factor defined as $s_A = A^{1/2}/(2\pi^{1/2}||v_1||^2)$ is related to the area A of the object, such that it becomes 1 for spherical shape. It shows a relative shape insensitivity for aspect ratios less than 5 and for flat structures. This shape factor has been used in isoperimetric inequalities to estimate the capacitance of objects with shapes close to the spherical shape²⁵.

The second scale-invariant shape factor related to capacitance is defined by $s_V = V^{1/3}/(\pi^{1/3}||v_1||^2)$. It is determined by the volume V of the object and shows shape insensitivity for long structures (Fig. 5). Thus for aspect ratios from 5 to 40 s_V is almost 1 for both rods and spheroids. In contrast to s_A , s_V varies not much for long structure, but it goes to 0 for flat structures.

These shape factors can be straightforwardly utilized in approximate capacitance calculations for metallic objects of various shapes. For instance, the capacitance for smooth shape approximants of the object can be calculated with the BIE method and then we may amend the

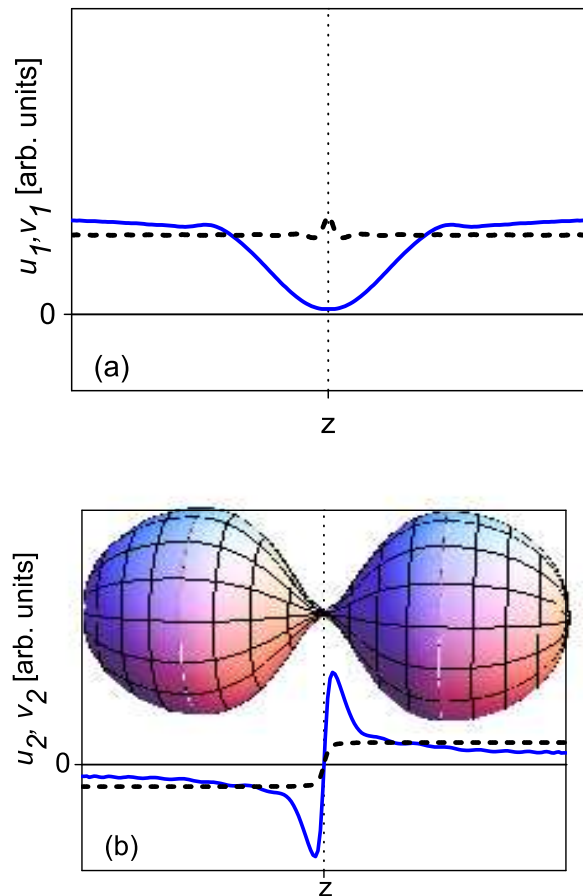


FIG. 6: (Color online) (a) The axial (z -) dependence of the first and (b) of the second eigfunctions of \hat{M} and \hat{M}^\dagger for a dimer; u_1 and u_2 are plotted with blue solid line, while v_1 and v_2 are depicted with black dashed lines. The inset of (b) shows the actual dimer.

final result with the appropriate area or volume by considering that the shape factor remains unchanged.

Our findings explain the $V^{1/3}$ scaling found for quantum capacitance of molecular nanowires³⁵, at least for the aspect ratios m from 5 to 30. For long rods, on the other hand, the volume V and the area A of the rod scale almost linearly with m . But the quantum capacitance is in fact proportional to $\ln(m)$ (see Ref. 35), which turns out to be quite close to $m^{1/3}$ for m between 5 and 30. This simple remark explains the $V^{1/3}$ scaling of quantum capacitance in the same range of aspect ratios. So, for long structures the volume plays a greater role in determining both classical and quantum capacitances.

An interesting case is that of a dimer with slightly connected metallic particles of nearly spherical shape^{22,23} with the shape depicted in the inset of Fig. 6b. In these systems the area and the volume related shape factors should become equivalent or close to that since they scale as R^2 and R^3 , respectively, R being the radius of the particles (the particles in the dimer are not quite

spheres but very close that). As a result the capacitance of the dimers scales with the radius of the constituent particles. Our numerical calculations show that both the area and the volume related shape factors are very close to 1, i. e., $s_A = 1.009$ and $s_V = 0.986$. Now we consider the case of two just touching spheres like that treated in Refs. 36,37, where analytical expressions of capacitance are provided. The capacitance of touching spheres is^{36,37}: $C_{dimer} = (2\ln 2) \times 4\pi\epsilon R \approx 1.386 \times 4\pi\epsilon R$. If we consider that $s_A = 1$ we obtain a capacitance $C_{dimerA} = 2^{1/2} \times 4\pi\epsilon R \approx 1.4142 \times 4\pi\epsilon R$. Similarly if $s_V = 1$ the capacitance is $C_{dimerV} = (8/3)^{1/3} \times 4\pi\epsilon R \approx 1.387 \times 4\pi\epsilon R$. It is easy to check that the two scale-invariant shape factors also reproduce with a good accuracy the results of the asymmetric dimers given in Ref. 36.

In dimers made of slightly connected particles many eigenfunctions of \hat{M} and \hat{M}^\dagger are hybrid eigenfunctions of the constituent particles^{22,23}. An example is provided in Figs. 6a and 6b, where the first two eigenfunctions of \hat{M} and \hat{M}^\dagger are plotted. The first eigenfunctions u_1 and v_1 of \hat{M} and \hat{M}^\dagger , respectively are basically symmetric combinations of the first eigenfunctions in the constituent particles. At the same time, the second eigenfunctions u_2 and v_2 are antisymmetric combinations of the same first eigenfunctions of the constituent particles. We notice that the first eigenmode u_1 provides the charging while it can not be a plasmon mode in metallic nanoparticles²³. In the space between the particles of the dimer the charge is repelled thus, the particles themselves repel each other (Fig. 6a). The second eigenmode, however, is a plasmon active mode in the long wavelength range²². Since the shape of v_2 is also constant on each particle, the first and the second eigenmode of \hat{M} lead to the reminiscence of $C(V, V)$ and $C(Q, -Q)$, respectively, when the particles of the dimer are separated^{36,38}. $C(V, V)$ is the capacitance when the two particles are kept at the same potential V and, at touching, turns into the dimer capacitance discussed above. In contrast, $C(Q, -Q)$ is the capacitance when the two particles are charged with opposite charges Q and $-Q$. It logarithmically diverges as the spheres approach the touching point^{36,38} since the charging mode transforms into a dipole-active mode. This behavior of $C(V, V)$ and $C(Q, -Q)$ is expected to hold for dimers of any shape as it has been recently found for ellipsoidal³⁹ or other, more general⁴⁰, shaped dimers. In addition, Fig. 6a is an illustrative image of sphere repulsion when they are in contact³⁷ and Fig. 6b provides a glimpse of sphere attraction when they are kept at a constant voltage difference^{37,38}.

D. Thin capacitors

Another application is the estimation of capacitance in thin capacitors like the membrane capacitance in living cells. The shelled ellipsoidal model and the spheroidal model, in particular, are two of the most common models of living cells used in modeling the dielectric spectroscopy

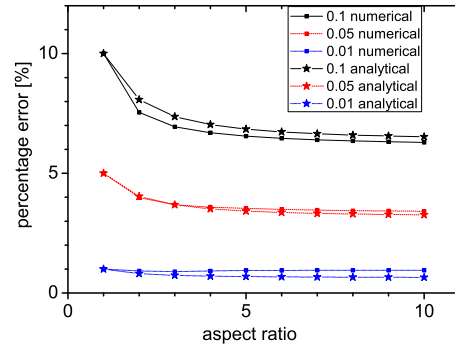


FIG. 7: (Color online) The percentage error of the planar-like capacitor formula with respect to the full numerical calculations (the square symbols) and with respect to analytical formula (the star symbols), i. e., Eq. (17), for thin constant-thickness spheroidal capacitors.

experiments. In the spheroidal shelled model the shell designates the cell membrane, which is practically non-conductive and bounded by two confocal spheroids. Both the spherical⁴¹ and the spheroidal⁴² models have analytical solutions for α - (below the frequency of 10 KHz) and β - (in the MHz range of the radiofrequency spectrum) relaxations⁴³. On the other hand, the membrane capacitance needs to be estimated as an input parameter in the analysis of α - and β -relaxations⁴¹. Eq. (13) gives us also an analytical form of the membrane capacitance in the spheroidal model, putting the ellipsoidal and the spherical models on the same footing in terms of solvability. However, realistic cell models would imply constant-thickness membrane, which is not found in the spheroidal model. In living cells, on the other hand, the membrane is very just a few tens of nm thick for a cell size in the μm range. Apparently, Eq. (9) is quite general for thin capacitors. The control parameter for accuracy is ζ_1 which is weighted by its Lamé coefficient. Thus, it is of great interest to look for the validity of (9) in the case of thin and constant-thickness capacitors.

We suppose that Σ_1 is sufficiently smooth and let us pick an arbitrary point \mathbf{r}_0 on Σ_1 that is locally parametrized by $\mathbf{r}(\zeta_1, \zeta_2)$ and consider its two principal directions in which the curvature tensor is diagonal. We assume without loss of generality that ζ_1 is the parameterization of the first principal direction and ζ_2 the parameterization of the second. We further assume that the unit tangent vectors are $\mathbf{t}_{1,2} = \frac{\partial \mathbf{r}}{\partial \zeta_{1,2}}$, such that the surface element is $d\Sigma_1 = d\zeta_1 d\zeta_2$. Hence, the unit normal vector on Σ_1 at \mathbf{r}_0 is $\mathbf{n} = \mathbf{t}_1 \times \mathbf{t}_2$. We also denote the curvature along the first principal direction at \mathbf{r}_0 as κ_1 and the curvature along the second principal direction at \mathbf{r}_0 as κ_2 . In this situation the constant-thickness capacitor is determined by Σ_1 and by Σ_2 that is defined as $\mathbf{r}'(\zeta_1, \zeta_2) = \mathbf{r}(\zeta_1, \zeta_2) + \delta a \mathbf{n}(\zeta_1, \zeta_2)$, where δa is the is

small and constant. Then the tangent vectors on Σ_2 are $\mathbf{t}'_{1,2} = \mathbf{t}_{1,2}(1 + \delta a \kappa_{1,2})$. Therefore, in the linear approximation with respect to δa , the surface element on Σ_2 is $d\Sigma_2 = d\zeta_1 d\zeta_2 (1 + 2\delta a H)$, with the mean curvature $H = (\kappa_1 + \kappa_2)/2$. The key approximation that comes under scrutiny is Eq. (10), which is valid as long as the electric field on Σ_2 is the same as the electric field on Σ_1 . According to the Gauss theorem the product of electric field and the surface element must be constant. In the linear approximation with respect to δa the field E_2 on Σ_2 is $E_2 = E_1(1 - 2\delta a H)$, where E_1 is the field on Σ_1 . Therefore, it is not hard to see that the voltage drop $V_1 - V_2$ must be amended by the factor $(1 - \delta a H)$ and Eq. (10) must be changed to

$$C_{\text{membrane}} = \varepsilon \frac{A}{\delta a} + \int_{y \in \Sigma_1} \varepsilon H d\Sigma_1(y). \quad (17)$$

Eq. (17) is a second order approximation of thin constant-thickness, where the first term on the right-hand side is the leading term. We have two straightforward consequences. First, Eq. (17) explains why the capacitance of cell membranes appear to be much larger whenever the membrane is folded⁴⁴. Second, it gives us also the validity criterion of parallel-plane capacitor-like formula which is $\delta a \int H d\Sigma_1(y)/A \ll 1$. In Fig. 7 we present the percentage error of the planar-like capacitor formula, Eq.(9), with respect to full numerical calculations and with respect to Eq. (17) for thin constant-thickness capacitors of prolate spheroidal shape. Three thicknesses are considered: 0.1, 0.05, and 0.01 of the largest axial cross-sectional radius of the spheroid. The calculations show that Eq. (17) is a good approximation of constant-thickness capacitors up to significant thicknesses. On the other hand, for extremely thin capacitors (a thickness of 0.01) the error of Eq.(9) is about 1%.

A useful application of Eq. (17) is the assessment of the geometry-dependent energy storage in supercapacitors. In a recent paper Huang et al.⁴⁵ noticed that the normalized capacitance (capacitance per unit area) of spherical and cylindrical double-layer capacitors increase with decreasing sphere and cylinder diameters. They also noticed that the capacitances of spherical capacitors increase faster than that of cylinders and argued that this behavior is related to the principal curvatures of those shapes⁴⁵. Eq. (17) provides not only the proof for the curvature-related capacitance but also a quantitative evaluation of shape dependent capacitance. In addition, the same equation can be utilized for double-layer capacitors of arbitrary shapes.

V. SUMMARY

In the second-kind integral equation based on the adjoint of the Neumann-Poincaré operator the capacitance as well as the static and dynamic polarizabilities can be simultaneously calculated for arbitrarily shaped objects. A compact capacitance formula is obtained and is simply stated as follows. The capacitance is direct proportional to the dielectric permittivity of the embedding medium and to the area of the object, and inverse proportional to the squared norm of the eigenfunction of the Neumann-Poincaré operator with the largest eigenvalue. A spectral based numerical implementation of the method is accurate and resembles the fast multipole method. Several applications are discussed. The capacitance formula allows us to define scale-invariant shape factors that varies slowly with shape and can be used in approximate calculations of capacitance. We have analyzed two scale-invariant shape factors. One of the shape factors employs the volume of the object and is more suitable for long shapes like rods or wires. The other shape factor, which is defined in terms of the object area, is more appropriate for objects with shapes close to a sphere. Both scale-invariant shape factors, however, provide an accurate capacitance of touching metallic dimers.

We have extended the above results to capacitors. More explicitly, we have considered a special class of capacitors defined by the equipotential surfaces of the equilibrium charge on an arbitrarily shaped body. In this case the capacitor behaves like a series capacitor with the total capacitance as being the capacitance of the inner surface in series with the opposite (negative) capacitance of the outer surface of the capacitor. This result leads to an integral form of capacitance that was used to estimate analytically the capacitance of confocal spheroidal capacitors and of finite cylinders. Another consequence is a second-order formula for thin constant-thickness capacitors of arbitrary shape. The first order term has a plane-capacitor like form, while the second order term is the surface integral of the mean curvature. Applications of a thin constant-thickness capacitor formula are encountered in the capacitance estimation of membrane in living cells and of supercapacitors with arbitrary shapes.

Acknowledgments

This work was supported by a grant of the Romanian National Authority for Scientific Research, CNCS – UEFISCDI, project number PNII-ID-PCCE-2011 -2-0069.

* Electronic address: titus.sandu@imt.ro

¹ O. D. Kellog, *Foundations of Potential Theory* (Springer-Verlag, Berlin-Heidelberg-New York, 1967).

² D. Khavinson, M. Putinar, and H. S. Shapiro, Arch. Ra-

tion. Mech. Anal. **185**, 143 (2007).

³ D. Vrinceanu and E. Gheorghiu, Bioelectrochem. Bioenerg. **40**, 167 (1996).

⁴ F. Ouyang and M. Isaacson, Philos. Mag. B **60**, 481 (1989).

- ⁵ I. D. Mayergoyz, D. R. Fredkin, and Z. Zhang, Phys. Rev. B **72**, 155412 (2005).
- ⁶ G. Robin, Ann. Sci. Ecole Norm. Sup. **3**, 1 (1886).
- ⁷ T. Simonson, Rep. Prog. Phys. **66**, 737 (2003).
- ⁸ W. A. Hofer, A. S. Foster, and A. L. Shluger, Rev. Mod. Phys. **75**, 1287 (2003).
- ⁹ A. Mottaghizadeh, P. L. Lang, L. M. Cui, J. Lesueur, J. Li, D. N. Zheng, V. Rebutini, N. Pinna, A. Zimmers, and H. Aubin, Appl. Phys. Lett. **102**, 053118 (2013).
- ¹⁰ P. Simon and Y. Gogotsi, Nature Mat. **7**, 845 (2008).
- ¹¹ J. F. Douglas, H. X. Zhou, and J. B. Hubbard, Phys. Rev. E **49**, 5319 (1994).
- ¹² M. Mascagnia and N. A. Simonov, J. Comput. Phys. **195**, 465 (2004).
- ¹³ C. Johnson, *Numerical Solutions of Partial Differential Equations by Finite Element Method* (Cambridge Univ. Press, Cambridge, 1987).
- ¹⁴ D. Poljak and C. A. Brebbia, *Boundary Element Methods for Electrical Engineers* (WIT, Boston, 2005).
- ¹⁵ V. Rokhlin, J. Comput. Phys. **60**, 187 (1985).
- ¹⁶ L. F. Greengard and V. Rokhlin, J. Comput. Phys. **73**, 325 (1987).
- ¹⁷ J. Tausch and J. White, Adv. Comput. Math. **9**, 217 (1998).
- ¹⁸ K. Nabors, F. T. Korsmeyer, F. T. Leighton, and J. White, SIAM J. Sci. Statist. Comput. **15**, 713 (1994).
- ¹⁹ A. Greenbaum, L. Greengard, and G. B. M. Fadden, J. Comput. Phys. **105**, 267 (1993).
- ²⁰ A. A. Farajian, O. V. Pupysheva, H. K. Schmidt, and B. I. Yakobson, Phys. Rev. B **77**, 205432 (2008).
- ²¹ T. Sandu, D. Vrinceanu, and E. Gheorghiu, Phys. Rev. E **81**, 021913 (2010).
- ²² T. Sandu, D. Vrinceanu, and E. Gheorghiu, Plasmonics **6**, 407 (2011).
- ²³ T. Sandu, Plasmonics **8**, 391 (2013).
- ²⁴ J. P. Boyd, *Chebyshev and Fourier Spectral Methods* (Dover, New York, 2001).
- ²⁵ Y. L. Chow and M. M. Yovanovich, J. Appl. Phys. **53**, 8470 (1982).
- ²⁶ L. D. Landau and E. M. Lifshitz, *Electrodynamics of Continuous Media* (Pergamon, Oxford-New York, 1984).
- ²⁷ O. D. Momoh, M. N. O. Sadiku, and C. M. Akujubi, Microw. Opt. Tech. Lett. **51**, 2361 (2009).
- ²⁸ M. L. Mansfield, J. F. Douglas, and E. J. Garboczi, Phys. Rev. E **64**, 061401 (2001).
- ²⁹ T. Sandu, J. Nanopart. Res. **14**, 905 (2012).
- ³⁰ W. R. Smythe, J. Appl. Phys. **33**, 2966 (1962).
- ³¹ J. D. Jackson, Am. J. Phys. **68**, 789 (2000).
- ³² C. M. Butler, J. Appl. Phys. **51**, 5607 (1980).
- ³³ J. C. Maxwell, Proc. London Math. Soc. **9**, 94 (1877).
- ³⁴ J. D. Jackson, Am. J. Phys. **70**, 409 (2002).
- ³⁵ J. C. Ellenbogen, C. A. Picconatto, and J. S. Burnim, Phys. Rev. A **75**, 042102 (2007).
- ³⁶ J. Lekner, J. Electrostat. **69**, 11 (2011).
- ³⁷ J. Lekner, Proc. R. Soc. A **468**, 2433 (2012).
- ³⁸ J. Lekner, J. Appl. Phys. **111**, 076102 (2012).
- ³⁹ T. Murovec and C. Brosseau, Appl. Phys. Lett. **102**, 084105 (2013).
- ⁴⁰ A. S. Khair, J. Appl. Phys. **114**, 134906 (2013).
- ⁴¹ E. Prodan, C. Prodan, , and J. H. Miller, Biophys. J. **95**, 4174 (2008).
- ⁴² A. D. Biasio, L. Ambrosone, and C. Cametti, Biophys. J. **99**, 163 (2010).
- ⁴³ R. Stoy, K. Foster, and H. Schwan, Phys. Med. Biol. **27**, 501 (1982).
- ⁴⁴ C. M. Lo, C. R. Keese, and I. Giaever, Biophys. J. **69**, 2800 (1995).
- ⁴⁵ J. Huang, B. G. Sumpter, V. Meunier, G. Yushin, C. Portet, and Y. Gogotsi, J. Mater. Res. **25**, 1525 (2010).